A robust and multifunctional calcium coordination polymer as selective fluorescent sensor for acetone and iron(+3) and as tunable proton conductor

Journal Name

A robust and multifunctional calcium coordination polymer as selective fluorescent sensor for acetone and iron (+3) and as tunable proton conductor

Zhao-Feng Wu,[a,b,#] Zhi-Hua Fu,[b,#] Ever Velasco,[a] Kai Xing,[c] Hao Wang,[d] Guo-Dong Zou,[e] Xiao-Ying Huang [b],* and Jing Li [a],*

A multifunctional calcium coordination polymer (Ca-CP) formulated as $[(CH_3)_2NH_2][Ca(Me_2tcpbH)(H_2O)]$ (**1**) has been synthesized and characterized. Compound **1** features a robust and novel three-dimensional (3D) network with cage-like cavities. The high thermal and moisture stability of the title compound makes it a good candidate for possible environment or energy related applications. Fluorescence (FL) studies demonstrate that **1** shows emission with a maximum at 350 nm under 270 nm excitation. The title compound acts as a selective and sensitive fluorescent sensor for the detection of acetone and Fe^{3+} ions at low concentrations. The FL intensity quenching percentage and the concentration ratio of Fe^{3+}/Fe^{2+} showed a linear relation with a Fe^{3+} concentration as low as 50 μM in Fe^{2+} aqueous solutions, offering an easy way to probe the extent of Fe^{2+} oxidation. Moreover, due to the relatively high hydration character of Ca^{2+}, the terminal water molecules and undeprotonated carboxylate groups form a strong hydrogen-bonded network within the structure, facilitating its tunable proton conduction under various humidity and temperatures. The proton conducting mechanism has been investigated by PXRD, IR, and EA methods.

1. Introduction

As a relatively new type of functional materials, coordination polymers (CPs) have become a hot topic in the past two decades, due to their structural tunability and promising applications in various fields, including but not limited to gas storage and separation, catalysis, and fluorescence-based chemical sensing.[1] Generally, CPs based on transition and post-transition metals, rare-earth metals, and main group metals such as zirconium, copper, zinc, yttrium, and aluminium have been well studied,[2] while alkaline earth (AE) metal based CPs are somewhat underexplored. In fact, the specific properties of the AE metals can endow AE-based CPs with unique characters, and

the investigation for AE-CPs may not only enrich the structure library of the CPs but also extend their applications.[3] For example, Mg^{2+} based CPs often possess comparatively high gravimetric gas storage capacities because of the low density of magnesium.[4] As a result of their strong Lewis acidity, AE-CPs show good performance in the base-catalyzed reactions.[5] Moreover, the economic and environmental advantages of AE metals, especially Mg^{2+} and Ca^{2+}, could facilitate CPs in future industrially applications. Therefore, designing AE^{2+} based CPs and exploring their applications are not only highly significant but also useful to the broader field of CPs chemistry.

Recently, we have focused our attention on designing fluorescent (FL) AE-CPs and we find both Mg^{2+} and Ca^{2+} are excellent candidates to construct FL CPs.[6] Due to the unique electron configuration of AE^{2+} ions, they are likely to form structures with linker-centred emission, simply by use of ligands with unique chromophoric properties. Recent studies have shown that such compounds exhibit comparative, and sometimes even higher, FL efficiency and better sensing performance when compared with the well-studied lanthanide or transition metal based FL CPs.[3c] In addition, AE^{2+} ions have relatively high hydration energies, and thus array of lattice or coordinated H_2O molecules are often contained in AE-CPs.[3b, 3c] The abundant hydrogen bonding networks could be constructed through the regular arrangement of these water molecules in the crystalline AE-CPs, enabling conduction of protons. As a result, AE-CPs may represent a promising type of

[a] *Department of Chemistry and Chemical Biology, 123 Bevier Rd. Piscataway, NJ 08854, United States*
[b] *State Key Laboratory of Structural Chemistry, Fujian Institute of Research on the Structure of Matter, the Chinese Academy of Sciences, Fuzhou, Fujian, 350002, P.R. China*
[c] *Harbin Institute of Technology, No.92 Xidazhi Street Nangang District, Harbin, 150006, P.R. China*
[d] *Hoffmann Institute of Advanced Materials, Shenzhen Polytechnic, Shenzhen, Guangdong 518055, P. R. China*
[e] *School of Chemistry & Chemical Engineering, Xinyang Normal University, Xinyang, Henan 464000, P.R. China*
[#] *The authors contributed equally.*
E-mail: jingli@rutgers.edu, xyhuang@fjirsm.ac.cn

materials for proton conduction. However, the high hydration character of the AE^{2+} metals, on the other hand, can also be a disadvantage leading to the poor moisture tolerance for AE-CPs and hinders their practical applications. Thus, designing robust AE-CPs with multi-functionalities remains challenging.

In this paper, we report a novel multifunctional Ca-CP with chemical formula $[(CH_3)_2NH_2][Ca(Me_2tcpbH)(H_2O)]$ (**1**, Me_2tcpbH_4 = 1,2,4,5-tetrakis(4-carboxyphenyl)-3,6-dimethyl-benzene). In structure **1**, four Me_2tcpbH bridge nine dimeric secondary building unit (SBU), $[Ca_2(COO)_8(H_2O)_2]$, to form a cage, which further connects the four neighboring cages to yield an anionic three dimensional (3D) framework with cage cavities. The deliberate use of Me_2tcpbH_4 with hydrophobe methyl groups as a bridging linker results in an unusually high thermal and moisture stability of the title compound. The FL measurements demonstrate that compound **1** exhibits selective and efficient FL sensing performance towards Fe^{3+} and acetone with high sensitivity. The linear relation between FL quenching percentage and the concentration ratio of Fe(III)/Fe(II) provide a convenient way to monitor the extent of Fe^{2+} oxidation. Moreover, due to the abundant hydrogen bonding network between the terminal water molecules and half deprotonated carboxylic group, **1** shows tunable proton conductivity with magnitude varying from 10^{-4} to 10^{-3} S/cm under different humidity and temperatures. The proton conducting mechanism was investigated by a number of analytical methods, including IR, EA and PXRD.

2. Experimental

2.1 Materials and methods
All the chemicals were used without further purification. Elemental analyses (EA) of C, H, and N were performed using a German Elementary Vario EL III instrument. Powder X-ray diffraction (PXRD) patterns were obtained from a Miniflex II diffractometer at 30 kV and 15 mA using Cu$K\alpha$ (1.54178 Å) in the angular range of 2θ = 3-35° at room temperature. Thermogravimetric data were collected on a TA Q5000 Analyzer with a temperature ramping rate of 10 °C min^{-1} from room temperature to 700 °C under a N_2 gas flow. The solid-state emission spectrum of the compound was recorded by a Duetta fluorescence and absorbance spectrometer at 298 K.

2.2 Synthesis
Synthesis of 1: A mixture of 50 mg Ca(ClO$_4$)$_2$·4H$_2$O and 20 mg Me_2tcpbH_4 in the mixed solvents of 5 mL DMF, 2 mL H$_2$O and 0.5 mL formic acid was sealed in a 20 mL glass vial and heated at 393 K for 2 days, followed by cooling to room temperature. The colorless block-like crystals were isolated after filtered, washed with ethanol for several times (Fig. S1) and dried at room temperature (0.030 g, 37% yield based on magnesium).

Synthesis of 1-T: The thermally treated sample was prepared by putting the as made crystals in an alumina crucible under N_2 atmosphere from 200 to 400 °C for 2 hours. Anal. Found. for **1-T** treated at 350°C for 2 hours: C, 22.07%; H, 1.79%; N, <0.3 %.

2.3 FL measurements

The as-made **1** was loaded into an agate mortar and was manually ground with a pestle to afford a fine powder. The FL was measured by dispersing 2 mg powder of **1** in 2 mL organic solvents or 2 mL 10^{-3} M metal solutions. The suspension was placed in a quartz cell of 1 cm-width for FL detection after ultrasonic treatment. Detailed detections for all titrants were carried out by gradually adding acetone and 10^{-3} M Fe^{3+} solution as quenchers in an incremental fashion. Pipette was utilized to add the quenchers into the emulsion for convenience of calculations of the sensing concentrations. The corresponding FL spectra were recorded on a Duetta fluorescence and absorbance spectrometer at room temperature. For all measurements, the dispersed solutions of **1** were excited at λ_{ex} = 270 nm (λ_{em} = 350 nm) and the corresponding emission wavelengths were monitored from 300 nm to 500 nm. The FL efficiency was calculated by $[(I_0-I)/I_0] \times 100\%$, where I_0 is the initial FL intensity.

2.4 X-ray crystallography
Crystal of **1** suitable for single crystal X-ray diffraction (SCXRD) was selected under an optical microscope and glued to a thin glass fiber. After data collection, the structure was solved by direct methods and refined with full-matrix least squares techniques using the *SHELX2016* package.[7] The detailed crystallographic data and structure-refinement parameters are summarized in Table 1.

Table 1 Crystallographic data and structural refinement details for **1**.

Empirical formula	$C_{38}H_{33}CaNO$
Crystal Size (mm)	0.24 x 0.22 x 0.22 mm
Crystal system	Orthorhombic
Space group	*Pbca*
a (Å)	20.4667(15)
b (Å)	10.3556(7)
c (Å)	32.400(2)
V (Å^3)	6867.0(8)
Z	8
μ (mm^{-1})	0.240
λ(MoKα) (Å)	0.71073
F(000)	2880
θ range (°)	2.292 to 27.138
Reflections measured	79184
Independent reflections	7580
Temperature (K)	100(2)
ρ_{calc}/g cm^{-3}	1.330
Parameter	458
R_{int}	0.0979
R_1,^{a} wR_2 [$I>2\sigma(I)$]^b	0.0441, 0.0957
R_1, wR_2 [all data]	0.0727, 0.1116
GOF	1.057
Largest diff. Peak and hole/e Å^{-3}	0.344 and -0.353

$^a R_1 = \sum \| F_o | - | F_c \| / \sum |F_o|$. $^b wR_2 = [\sum w(F_o{}^2 - F_c{}^2)^2 / \sum w(F_o{}^2)^2]^{1/2}$

2.5 Proton conductivity measurements

The proton conductivity measurements were performed by quasi-four-electrode alternating current (AC) impedance technique using a Solartron 1260 impedance/gain-phase analyzer. The powdered samples were compressed to pellets under a pressure of 101 MPa. Two sides of the pellet were connected to gold wires by gold paste. The sample pellet was measured at frequency ranging from 10^7 to 1 Hz by varying temperature from 30 to 80 °C and relative humidity (RH) from 40 to 98%. The conductivity of the sample was deduced from the Debye semicircle in Nyquist plot.

3. Results and discussion
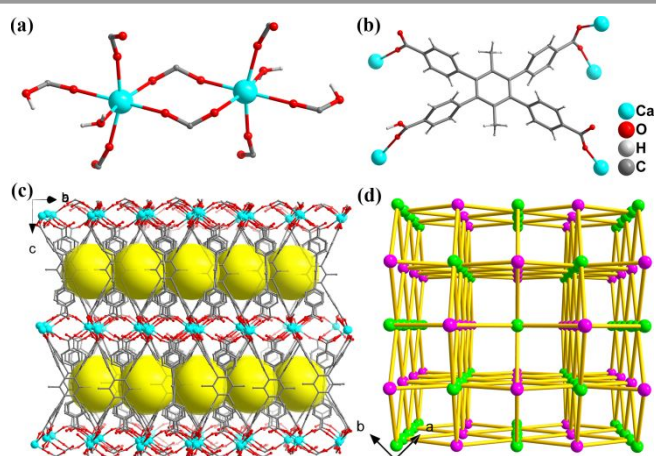
3.1 Crystal structure description

Fig. 1 (a) The coordination environment for Ca^{2+}. (b) The ligand coordination mode in **1**. (c) The 3D structure of **1** viewed along the *a* axis. Hydrogen atoms and $[(CH_3)_2NH_2]^+$ are omitted for clarity. (d) The topology of **1**.

Single-crystal X-ray diffraction result indicates **1** features a 3D structure belonging to the space group of *Pbca*. The asymmetric unit of **1** contains one crystallographically unique Ca^{2+} ion, one Me_2tcpbH ligand, one terminal H_2O and one $[(CH_3)_2NH_2]^+$ cation. As depicted in Fig. 1a, the Ca^{2+} is octahedrally coordinated by five oxygen atoms from five carboxylic groups, including four COO^- and one unprotonated COOH groups through a monodentate coordination mode, and the last coordination site is occupied by the terminal H_2O molecule. Such two Ca^{2+} ions are connected by two carboxylic groups to form a dimer of $[Ca_2(COO)_8(H_2O)_2]^{4-}$ acting as the SBU for **1**. The Ca–O lengths fall in the range of 2.3107(15) and 2.3510(15) Å. Each dimer SBU is bridged by the Me_2tcpbH ligand with one coordination mode to form a novel 3D framework with cage cavities viewed along the *a* axis, Figs. 1b and 1c. The cage highlighted by yellow ball is made of four Me_2tcpbH ligands bridging nine dimer SBUs (Fig. S3). However, due to the existence of the methyl group in the Me_2tcpbH ligand, the access from one cage to the adjacent one is blocked, Fig. S3. From the topological point of view, **1** possess a $\{4^4.6^2\}^2\{4^8.6^{16}.8^4\}$ topology built upon 4, 8-connected net, Fig. 1d. As shown in Fig. S4, the hydrogen bonding exists between

the carboxylic oxygen atoms and H atoms in the terminal water, dimethylamine cations produce an abundant H-bonding network in **1** (Table S1).
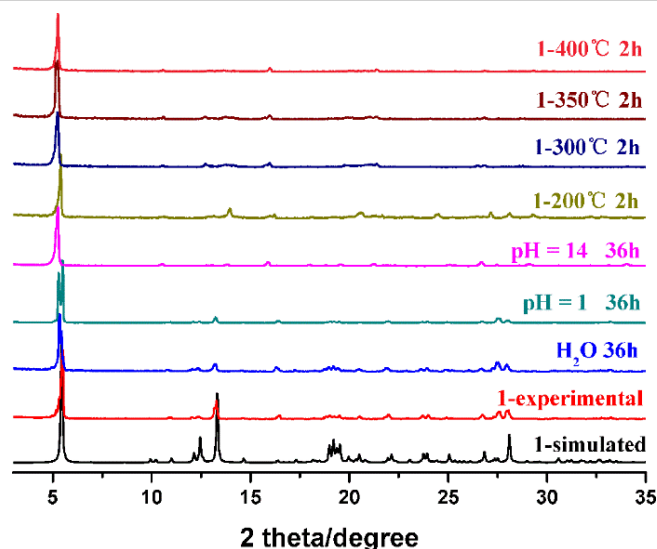
3.2 FL sensing properties

Fig. 2 PXRD patterns of as-made sample of **1** under different conditions.
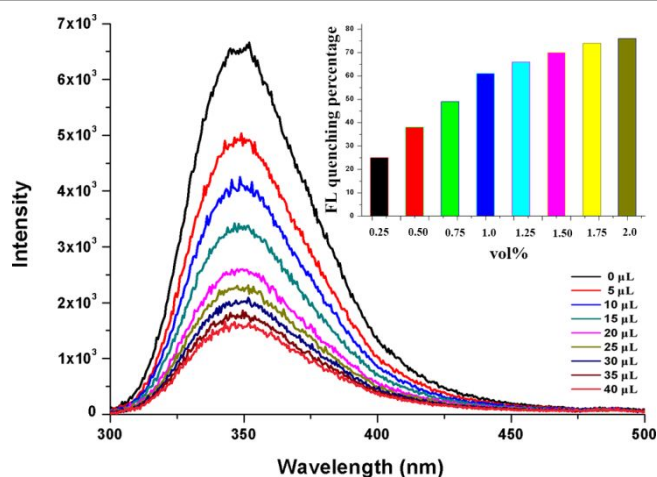

Fig. 3 FL spectra of **1** upon addition of various volumes of acetone. Inset is FL quenching percentage of **1** as a function of volume percentages of acetone.

The stability of the title compound was evaluated under different conditions. As shown in Fig. 2, PXRD patterns of the samples under the pH values of 1 and 14 for 36 h are nearly identical to the as-made one, indicating high resistance of **1** under aqueous and acidic-basic environment. PXRD analysis also demonstrated high stability of the samples under heating over a wide temperature range from 200 to 400 °C, Fig. 2. The excellent thermal and water stabilities of the title compound prompted us to explore its potential for sensing applications. As depicted in Fig. S6a, at room temperature, **1** emits UV light in the solid state with a maximum at 350 nm under excitation wavelength of 270 nm. Compared with the emission spectrum of the ligand Me_2tcpbH_4 (Fig. S6b) it is clear that the fluorescence of the title compound is a ligand centered emission. When a powdered sample was dispersed in the commonly used solvents, the FL intensity of **1** in

acetone exhibited the most quenching effect, indicating its selective sensing to acetone, Fig. S7. To quantitatively measure the sensing sensitivity of **1** for acetone, a powdered sample was then ultrasonically dispersed in H_2O to form a stable emulsion. The quenching percentage of FL intensity was recorded as a function of volume percentage of acetone added to the emulsion of **1**. As seen in Fig. 3, the FL intensity was quenched more than 60% when only 1.0 volume percentage of acetone was added (inset of Fig. 3), demonstrating an excellent sensitivity of **1** towards acetone. From the Stern-Volmer equation: $I_0/I = 1 + K_{sv} \times [M]$,[8] the K_{sv} value was calculated to be 1.24×10^4 L·mol^{-1}, Fig. S8. The limit of detection (LOD) for acetone was 3.12 mM calculated from the ratio of 3δ/slope. The LOD value is comparable with those of transition metal or rare earth metal based FL CPs reported to this date,[9] as shown in Table S2. It is worth to mention that compound **1** represents the first AE metal based CP for acetone detection.
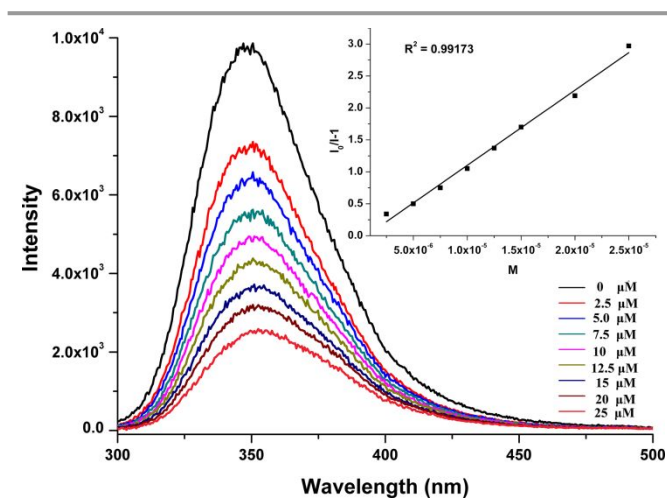
quenching effect while Fe^{3+} almost totally quenched FL of **1**. To quantitatively monitor the quenching performance, 2 mg powder of compound **1** was dispersed in 2 mL H_2O. The quenching percentage was recorded as a function of increasing amount of 10^{-3} M Fe^{3+} ions added to the emulsion, Fig. 4. The FL was quenched more than 50% only at a concentration of 10 μM Fe^{3+} ions. As shown in the inset of Fig. 4, the SV plot displays a good linear behavior with $R^2 = 0.99173$ and the K_{sv} value was calculated to be 1.18×10^5 L·mol^{-1}. Compared with the reported values, the K_{sv} of **1** is among the most sensitive CP sensors for Fe^{3+} detection,[10] Table S3. Again, compound **1** represents the first Ca-CP FL sensor for Fe^{3+}. The LOD was obtained as 20.85 μM from the ratio of 3δ/slope. As seen in Table S3, most of the reported FL CP sensors for Fe^{3+} use organic solvents as dispersing media due to their poor hydrolytic stabilities, while the uncommon water tolerance of **1** makes it a good candidate as FL sensor of Fe^{3+} in water.

It is well known that Fe^{2+} can easily be oxidized to Fe^{3+} without special protection. Thus, seeking for an easy way to quantitatively determine the amount of Fe^{3+} in Fe^{2+} is meaningful. Compound **1** demonstrates such a capability, allowing conveniently monitoring the ratio of Fe^{3+} in Fe^{2+}. As seen in Fig. 5, when 10^{-3} M Fe^{3+} was added to the emulsion of **1** dispersed in 10^{-3} M Fe^{2+} solution, its FL intensity was decreased gradually with increasing concentration of Fe^{3+}. The FL quenching percentage shows a good linear relation with the concentration of Fe^{3+} in Fe^{2+} ($R^2 = 0.99274$), indicating **1** can act as a FL sensor to monitor the extent of oxidation of Fe^{2+} in the solution.

Fig. 4 FL spectra of **1** upon addition of various amounts of 10^{-3} M Fe^{3+}. Inset is the corresponding K_{sv} curve.

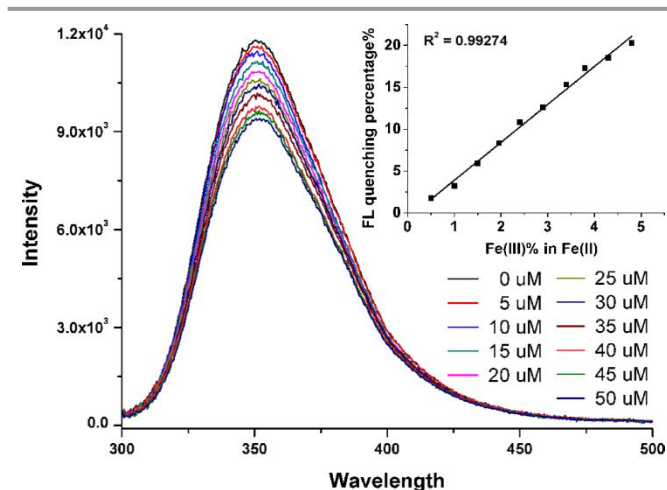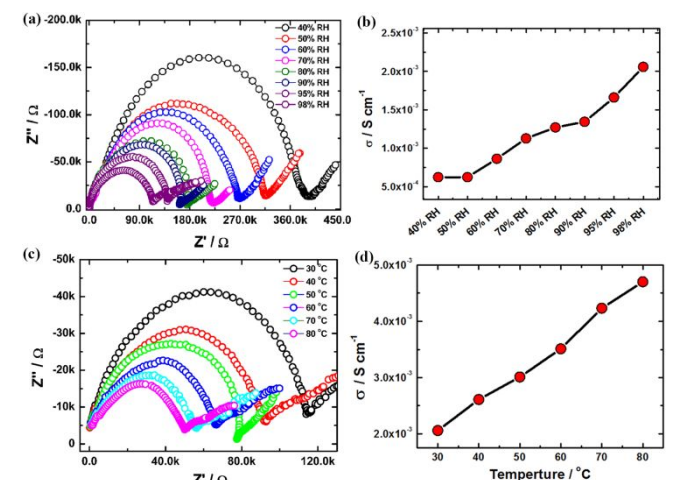**Fig. 5** FL spectra of **1** (dispersed in 10^{-3} M Fe^{2+} solution) upon addition of various amounts of 10^{-3} M Fe^{3+}. Inset is the plot of FL quenching percentage as a function of Fe(III)/Fe(II)%.

The selectivity of **1** towards different metal ions was examined by dispersing powered samples in various 10^{-3} M solutions of M(NO$_3$)$_n$ (M = Li$^+$, Na$^+$, K$^+$, Mg^{2+}, Ca^{2+}, Zn^{2+}, Cd^{2+}, Pb^{2+}, Hg^{2+}, Fe^{2+}, Al^{3+}, Fe^{3+}). As depicted in Fig. S9, most of the metal ions only showed mild

Fig. 6 (a) Nyquist plots for **1** at 30 °C under 40 to 98% RH. (b) Proton conductivity (σ) values of **1** under different humidity conditions. (c) Nyquist plots for **1** at 98% RH varied from 30 to 80 °C. (d) σ values of **1** at different temperatures.

3.3 Proton conducting properties

Proton conducting materials have recently received tremendous attention. Generally, proton conducting materials contain proton carriers such as imidazole, sulfonate, and phosphonate, to name a few.[11] Additionally, hydrogen bonding networks as proton conducting pathways also significantly improve proton conductivity (σ) of the materials. AE ions have relative high hydration energies, and H_2O molecules are often contained in AE-CPs as terminal ligands,[3b, 3c] thus, forming strong H-bonding networks. For example, the hydration ions

$(Mg(H_2O)_6)^{2+}$ confined in a 2D $[Mg(H_2O)_6][NaFe(C_2O_4)_3] \cdot 3H_2O$ endow it with good proton conductivity with $\sigma = 3 \times 10^{-3}$ S cm^{-1} at 298 K and 90% relative humidity (RH);[12] Ca-PiPhtA (PiPhtA = (dihydroxyphosphoryl) isophthalic acid) with abundant coordinated H_2O and lattice water (five H_2O per unit cell) exhibits 6.6×10^{-3} S cm^{-1} conductivity at 24 °C and 98% RH;[13] $Mg_2(H_2O)_4(H_2L) \cdot H_2O$ (H_6L = 2,5-dicarboxy-1,4-benzene-diphosphonic acid) with a strong H-bonding network shows high conductivity of 3.55×10^{-2} S cm^{-1} at 70 °C and 95% RH.[14] However, proton conductive AE-CPs remain relatively rare compared with the transition metal based CPs such as Zr-CPs.[13-15] Since **1** contains $[(CH_3)_2NH_2]^+$ cations and a strong H-bonding network (Fig. S4), we speculate that it may be a good proton conducting material. With this in mind, the proton conductivity of **1** was evaluated on an AC impedance/gain-phase analyzer using compacted pellet of the powdered **1** under various RH levels and temperatures. As shown in Fig. 6a, the Nyquist plots indicate the humidity dependent proton conductivities of **1**. When the RH values were changed from 40 to 98%, the conductivity of **1** gradually increased from 6.25×10^{-4} S cm^{-1} to 2.06×10^{-3} S cm^{-1}, Fig. 6b. The pellet also exhibited temperature dependent proton conducting behaviour, as shown in Figs. 6c and 6d. Along with the increase of temperature from 30 to 80 °C, the σ values increased from 2.06×10^{-3} S cm^{-1} to 4.70×10^{-3} S cm^{-1} at 98% RH, more than a twofold improvement (Fig. 6d). As depicted in Fig. S10, the activation energy of proton conductivity for **1** is 0.18 eV, indicating the Grotthuss transfer mechanism via water molecules (0.1 ~ 0.5 eV).[16]

The IR and EA analyses were carried out to further understand the proton conducting mechanism. Compound **1** was treated under 350 °C for 2 hours (**1-T**) and its proton conducting performance was investigated. The PXRD patterns of the sample under various acidity, after thermal treatment and proton conduction measurements match well with that of the as-made sample, indicating that crystallinity and structure remain unchanged under these conditions (Figs. 2 and Fig. S11). The IR spectra of **1** and **1-T** are shown in Fig. S12, and the results confirm the characteristic peak for C-N is weakened in **1-T** compared with that of the as-made sample. From the elemental analysis the N content ($<$0.3%) in **1-T** is much lower than that of the as-made sample **1** (4.2%), further revealed the partial decomposition of $[(CH_3)_2NH_2]^+$ cation upon heating. As seen in Fig. S13, under different RH values from 40 to 98%, the proton conductivity of **1-T** gradually increases from 4.78×10^{-6} S cm^{-1} to a maximum value of 4.80×10^{-4} S cm^{-1}. Compared with the as-made sample, the conductivity of **1-T** decreased by one order of magnitude. The result indicates that $[(CH_3)_2NH_2]^+$ cations act as proton carriers and H-donors for H-bonding network and, therefore, played an important role in proton conducting. At 98% RH condition, the performance of **1-T** was enhanced significantly with the increase of temperature. The maximum conductivity is 1.28×10^{-3} S cm^{-1} under 80 °C, Fig. S14. However the value is fourfold lower than that of **1** under the same conditions. This result suggests that without the $[(CH_3)_2NH_2]^+$ cation as proton carrier, the proton transfer in **1-T** is limited due to the lack of energy. The higher activation energy of 0.22 eV for **1**-T, compared to 0.18 eV for **1**, further verifies this

conclusion (Fig. S15). All the results mentioned above indicate both the regular H-bonding nework and the type of the proton carrier should be taken into consideration when designing materials with good proton conducting performance.

4. Conclusions

In summary, a novel multifunctional 3D AE-CP based on Ca^{2+} cations, $[(CH_3)_2NH_2][Ca(Me_2tcpbH)(H_2O)]$, has been designed, synthesized and characterized. The title compound shows an ultrahigh thermal and water stability, making it a good candidate for selective FL sensing of Fe^{3+} and acetone with high sensitivity. Moreover, due to the abundant H-bonding network and $[(CH_3)_2NH_2]^+$ cation acting as proton transfer pathway and proton carrier, respectively, compound **1** exhibits good and tunable proton conductivity at different humidity and temperatures. Our future work will continue to be focusing on the development of more stable AE-CPs with multi-functionalities and enhanced performance.

Acknowledgements

Conflicts of interest

There are no conflicts to declare.

Notes and references

1. (a) L. Q. Ma, C. Abney and W. B. Lin, *Chem. Soc. Rev.*, 2009, **38**, 1248; (b) L. J. Murray, M. Dinca and J. R. Long, *Chem. Soc. Rev.*, 2009, **38**, 1294; (c) Y. J. Cui, Y. F. Yue, G. D. Qian and B. L. Chen, *Chem. Rev.*, 2012, **112**, 1126; (d) P. Horcajada, R. Gref, T. Baati, P. K. Allan, G. Maurin, P. Couvreur, G. Férey, R. E. Morris and C. Serre, *Chem. Rev.*, 2012, **112**, 1232; (e) Y. J. Cui, B. Li, H. J. He, W. Zhou, B. L. Chen and G. D. Qian, *Acc. Chem. Res.*, 2016, **49**, 483; (f) B. Y. Li, M. Chrzanowski, Y. M. Zhang and S. Q. Ma, *Coord. Chem. Rev.*, 2016, **307**, 106; (g) L. Wang, Y. Z. Han, X. Feng, J. W. Zhou, P. F. Qi and B. Wang, *Coord. Chem. Rev.*, 2016, **307**, 361; (h) N. S. Bobbitt, M. L. Mendonca, A. J. Howarth, T. Islamoglu, J. T. Hupp, O. K. Farha and R. Q. Snurr, *Chem. Soc. Rev.*, 2017, **11**, 3357.

2. (a) D. J. Tranchemontagne, J. L. Mendoza-Cortes, M. O'Keeffe and O. M. Yaghi, *Chem. Soc. Rev.*, 2009, **38**, 1257; (b) J. Rocha, L. D. Carlos, F. A. A. Paz and D. Ananias, *Chem. Soc. Rev.*, 2011, **40**, 926; (c) J. Heine and K. Muller-Buschbaum, *Chem. Soc. Rev.*, 2013, **42**, 9232; (d) M. Eddaoudi, D. F. Sava, J. F. Eubank, K. Adil and V. Guillerm, *Chem. Soc. Rev.*, 2015, **44**, 228; (e) Y. Bai, Y. B. Dou, L. H. Xie, W. Rutledge, J. R. Li and H. C. Zhou, *Chem. Soc. Rev.*, 2016, **45**, 2327; (f) G. Calvez, F. Le Natur, C. Daiguebonne, K. Bernot, Y. Suffren and O. Guillou, *Coord. Chem. Rev.*, 2017, **340**, 134.

3. (a) K. M. Fromm, *Coord. Chem. Rev.*, 2008, **252**, 856; (b) D. Banerjee and J. B. Parise, *Cryst. Growth Des.*, 2011, **11**, 4704; (c)

Z. F. Wu, B. Tan, W. P. Lustig, E. Velasco, H. Wang, X. Y. Huang and J. Li, *Coord. Chem. Rev.*, 2019, **399**; (d) T. Xiao and D. Liu, *Microporous Mesoporous Mater.* 2019, **283**, 88..

4. (a) W. Zhou, H. Wu and T. Yildirim, *J. Am. Chem. Soc.*, 2008, **130**, 15268; (b) H. Wu, W. Zhou and T. Yildirim, *J. Am. Chem. Soc.*, 2009, **131**, 4995; (c) R. B. Getman, Y. S. Bae, C. E. Wilmer and R. Q. Snurr, *Chem. Rev.*, 2012, **112**, 703; (d) K. Sumida, D. L. Rogow, J. A. Mason, T. M. McDonald, E. D. Bloch, Z. R. Herm, T. H. Bae and J. R. Long, *Chem. Rev.*, 2012, **112**, 724.

5. (a) M. F. Ingleson, J. P. Barrio, J. Bacsa, A. Steiner, G. R. Darling, J. T. A. Jones, Y. Z. Khimyak and M. J. Rosseinsky, *Angew. Chem. Int. Ed.*, 2009, **48**, 2012; (b) A. E. P. Prats, V. A. de la Pena-O'Shea, M. Iglesias, N. Snejko, A. Monge and E. Gutierrez-Puebla, *ChemCatChem*, 2010, **2**, 147; (c) D. Saha, T. Maity and S. Koner, *Dalton Trans.*, 2014, **43**, 13006; (d) F. L. Liu, Y. W. Xu, L. M. Zhao, L. L. Zhang, W. Y. Guo, R. M. Wang and D. F. Sun, *J. Mater. Chem. A*, 2015, **3**, 21545.

6. (a) Z. F. Wu, B. Tan, M. L. Feng, A. J. Lan and X. Y. Huang, *J. Mater. Chem. A*, 2014, **2**, 6426; (b) Z. F. Wu, B. Tan, J. Y. Wang, C. F. Du, Z. H. Deng and X. Y. Huang, *Chem. Commun.*, 2015, **51**, 157; (c) Z. F. Wu, B. Tan, Z. L. Xie, J. J. Fu and X. Y. Huang, *J. Mater. Chem. C*, 2016, **4**, 2438; (d) Z. F. Wu, B. Tan, L. K. Gong, X. Zhang, H. Wang, Y. Fang, X. Z. Hei, Z. Z. Zhang, G. Y. Zhang, X. Y. Huang and J. Li, *J. Mater. Chem. C*, 2018, **6**, 13367; (e) Z. F. Wu, E. Velasco, C. Shan, K. Tan, Z. Z. Zhang, Q. Q. Hu, K. Xing, X. Y. Huang and J. Li, *J. Mater. Chem. C*, 2020, **8**, 6820.

7. G. M. Sheldrick, Crystal Structure Refinement with SHELXL, *Acta Crystallogr., Sect. C: Struct. Chem.* 2015, **71**, 3-8.

8. (a) J. C. Sanchez and W. C. Trogler, *J. Mater. Chem.*, 2008, **18**, 3143; (b) J. C. Sanchez, S. A. Urbas, S. J. Toal, A. G. DiPasquale, A. L. Rheingold and W. C. Trogler, *Macromolecules*, 2008, **41**, 1237.

9. (a) B. Chen, Y. Yang, F. Zapata, G. Lin, G. Qian and E. B. Lobkovsky, *Adv. Mater.*, 2007, **19**, 1693; (b) Z. Guo, H. Xu, S. Su, J. Cai, S. Dang, S. Xiang, G. Qian, H. Zhang, M. O'Keeffe and B. Chen, *Chem. Commun.*, 2011, **47**, 5551; (c) J.-M. Zhou, W. Shi, N. Xu and P. Cheng, *Inorg. Chem.*, 2013, **52**, 8082; (d) Q. Zhang, J. Wang, A. M. Kirillov, W. Dou, C. Xu, C. Xu, L. Yang, R. Fang and W. Liu, *ACS Appl. Mater. Interfaces*, 2018, **10**, 23976; (e) T. Gao,

B.-X. Dong, Y. Sun, W.-L. Liu and Y.-L. Teng, *J. Mater. Sci.*, 2019, **54**, 10644; (f) J. Zhang, S. B. Peh, J. Wang, Y. Du, S. Xi, J. Dong, A. Karmakar, Y. Ying, Y. Wang and D. Zhao, *Chem. Commun.*, 2019, **55**, 4727; (g) B. Zhu, Z. Zong, X. Zhang, D. Zhang, L. Cui, C. Bi and Y. Fan, *Appl. Organometal. Chem.*, 2020, **34**, e5518.

10. (a) Y.-J. Yang, M.-J. Wang and K.-L. Zhang, *J. Mater. Chem. C*, 2016, **4**, 11404; (b) W. Yan, C. Zhang, S. Chen, L. Han and H. Zheng, *ACS Appl. Mater. Interfaces*, 2017, **9**, 1629; (c) L. Liu, Y. Wang, R. Lin, Z. Yao, Q. Lin, L. Wang, Z. Zhang and S. Xiang, *Dalton Trans.*, 2018, **47**, 16190; (d) J.-H. Wei, J.-W. Yi, M.-L. Han, B. Li, S. Liu, Y.-P. Wu, L.-F. Ma and D.-S. Li, *Chem. Asi. J.*, 2019, **14**, 3694; (e) B. B. Rath and J. J. Vittal, *Inorg. Chem.*, 2020, **59**, 8818; (f) Y. e. Yu, Y. Wang, H. Yan, J. Lu, H. Liu, Y. Li, S. Wang, D. Li, J. Dou, L. Yang and Z. Zhou, *Inorg. Chem.*, 2020, **59**, 3828.

11. (a) W.-H. Wang, Q. Gao, A.-L. Li, Y.-Y. Jia, S.-Y. Zhang, J.-H. Wang, Y.-H. Zhang and X.-H. Bu, *Chin. Chem. Lett.*, 2018, **29**, 336; (b) D.-W. Lim and H. Kitagawa, *Chem. Rev.*, 2020, DOI: 10.1021/acs.chemrev.9b00842; (c) Y. X. Ye, L. S. Gong, S. C. Xiang, Z. J. Zhang and B. L. Chen, *Adv. Mater.*, 2020, **32**, 1907090.

12. I. Huskić, N. Novendra, D.-W. Lim, F. Topić, H. M. Titi, I. V. Pekov, S. V. Krivovichev, A. Navrotsky, H. Kitagawa and T. Friščić, *Chem. Sci.*, 2019, **10**, 4923.

13. M. Bazaga-Garcia, R. M. P. Colodrero, M. Papadaki, P. Garczarek, J. Zon, P. Olivera-Pastor, E. R. Losilla, L. Leon-Reina, M. A. G. Aranda, D. Choquesillo-Lazarte, K. D. Demadis and A. Cabeza, *J. Am. Chem. Soc.*, 2014, **136**, 5731.

14. P. Ramaswamy, N. E. Wong, B. S. Gelfand and G. K. H. Shimizu, *J. Am. Chem. Soc.*, 2015, **137**, 7640.

15. (a) R. M. P. Colodrero, P. Olivera-Pastor, E. R. Losilla, D. Hernandez-Alonso, M. A. G. Aranda, L. Leon-Reina, J. Rius, K. D. Demadis, B. Moreau, D. Villemin, M. Palomino, F. Rey and A. Cabeza, *Inorg. Chem.*, 2012, **51**, 7689; (b) T. Kundu, S. C. Sahoo and R. Banerjee, *Chem. Commun.*, 2012, **48**, 4998; (c) S. S. Park, A. J. Rieth, C. H. Hendon and M. Dincă, *J. Am. Chem. Soc.*, 2018, **140**, 2016.

16. (a) A. T. Howe and M. G. Shilton, *J. Solid State Chem.*, 1980, **24**, 149; (b) L. Bernard, A. Fitch, A. F. Wright, B. E. F. Fender and A. T. Howe, *Solid State Ionics*, 1981, **5**, 459; (c) S. Cukierman, *Bba-Bioenergetics*, 2006, **1757**, 876.

TOC

A robust and multifunctional calcium coordination polymer as selective fluorescent sensor for acetone and iron (+3) and as tunable proton conductor

Zhao-Feng Wu,[a,b,#] Zhi-Hua Fu,[b,#] Ever Velasco,[a] Kai Xing,[c] Hao Wang,[d] Guo-Dong Zou,[e] Xiao-Ying Huang [b,*] and Jing Li [a,*]
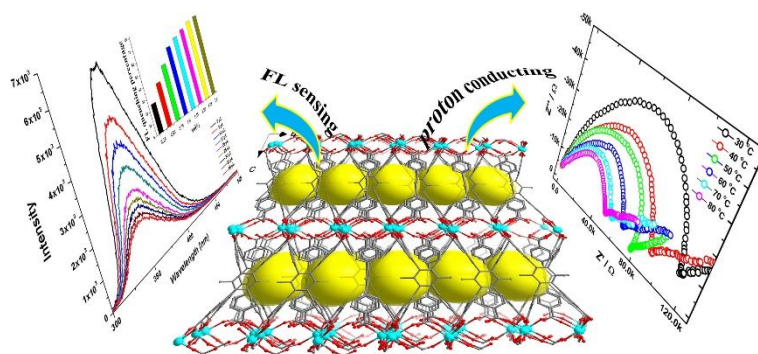
A robust 3D Ca-CP demonstrates selective fluorescence-based sensing of Fe^{3+} and acetone as well as tunable proton conduction.